Radio Science, Volume 35, Number 1, Pages 179–193, January–February 2000

Tropospheric measurements of turbulence and characteristics of Bragg scatterers using the Jicamarca VHF radar

Jorge L. Chau[1]

Radio Observatorio de Jicamarca, Instituto Geofísico del Perú, Lima

Richard J. Doviak

NOAA National Severe Storms Laboratory, Norman, Oklahoma

Andreas Muschinski

CIRES, University of Colorado, and NOAA Environmental Technology Laboratory, Boulder, Colorado

Christopher L. Holloway

Institute for Telecommunication Sciences, National Telecommunications and Information Administration, Boulder, Colorado

Abstract. We apply the *Holloway et al.* [1997a] spaced antenna (SA) method to data collected with the Jicamarca VHF radar. Measurements are presented of an indicator of turbulent intensity (i.e., the standard deviation of the velocity fluctuation) and the parameters (orientation and correlation lengths) of horizontally anisotropic Bragg scatterers at tropospheric heights. We compare SA indicators of turbulence intensity to concurrent measurements obtained with a very narrow vertical beam ($\sim$0.8°). This comparison results in a very good agreement. We also show that the Jicamarca observations are due to a Fresnel scattering mechanism rather than a reflecting one. Finally, we find an L-shaped regression between the correlation lengths of Bragg scatterers and the indicators of turbulent intensity. When turbulence is weak ($\sigma_t < 0.1$ m s^{-1}), the horizontal correlation lengths have a large spread of relatively large values (i.e., large aspect sensitivity), but when turbulence is strong, the horizontal correlation lengths are much smaller.

1. Introduction

In this paper we apply the spaced antenna (SA) method described by *Holloway et al.* [1997a] (hereinafter referred to as Holloway et al.) to data collected with the Jicamarca VHF radar to determine the size, shape, and orientation of Bragg scatterers in the troposphere and to relate these characteristics of stochastic Bragg scatter [*Doviak*, 1999] to levels of turbulence in the flow and the location of scatterers relative to the radar site. Although Holloway et al. assume a Gaussian correlation model to simplify the solution, it can be shown, using results of *Doviak et al.* [1996], that the formulas of Holloway et al. can be extended to stochastic Bragg scatter from refractive index perturbations best described by a spectral model that includes both the anisotropic and isotropic characteristics of the scatterers. In this spectral model the isotropic characteristics are those associated with perturbations of refractive index calculated from the accepted Kolmogorov theory of turbulence. This is the first time

[1]Also at Laboratorio de Física, Universidad de Piura, Piura, Perú.

Paper number 1999RS002163.
0048-6604/00/1999RS002163$11.00

that the Jicamarca radar was used in the SA mode to observe the characteristics of the scatterers and turbulence in the tropospheric region. We estimate the levels of turbulence and use statistical methods to infer the accuracy of these estimates. We use the uniquely narrow beam of the Jicamarca radar (~0.8° half-power beam width) to calculate directly the levels of turbulence without having to correct for beam-broadening effects because they are expected to be very small [e.g., *Hocking*, 1996]. For example, for an isotropic atmosphere and a 5 m s^{-1} horizontal wind (typical value over Jicamarca between 5 and 10 km) the beam-broadening contribution is $\leq$2.34 cm s^{-1}. The narrow beam turbulence estimates are compared with those determined by the SA method.

The Holloway et al. method to determine the cross correlation of signals in spaced receivers is based upon a model of the statistical characteristics of the scatterers and the flow in which they are embedded. However, the cross-correlation functions reduce exactly to those derived from the full correlation analysis (FCA) of *Briggs* [1984, equation (12)] and *Briggs and Vincent* [1992, equation (32)], which are principally based on models of the diffraction pattern. Furthermore, Holloway et al.'s approach explicitly accounts for the effects that the transmitting and receiving antennas have on the diffraction patterns, whereas in a generalized FCA [*Briggs*, 1992] these effects are only implicitly expressed. Also, using the results of *Doviak et al.* [1996], Holloway et al.'s approach can be applied to scattering from refractive index perturbations in turbulent flow described by the Kolmogorov theory of turbulence.

Holloway et al.'s formulation and therefore those derived from FCA apply to receivers symmetrically placed about the transmitter. Recently, *Holloway et al.* [1998] have presented emendations to the Holloway et al.'s formulas to consider general SA configurations. These corrections do not change significantly the magnitude of cross-correlation functions, but the phase component could be significantly modified, affecting vertical velocity and angle of arrival measurements. These phase terms have been studied in more detail by *Chau and Balsley* [1998a].

The Jicamarca data set that we use in this work has been obtained using a noncollocated SA configuration (i.e., receivers are not symmetrically placed about the transmitter). Because the horizontal wind vector, turbulence, and Bragg scatterers' sizes, shape, and orientation (i.e., the parameters of the scatterers' horizontal correlation ellipse) depend only on the magnitude of the cross-correlation and autocorrelation functions; the measurements of these variables are not affected by the noncollocated SA configuration.

Hocking and Hamza [1997] point out that earlier reports of experiments simply classify the scatterers as "specular" and "isotropic". In the appendix, we use quantitative theory [e.g., *Doviak and Zrnić*, 1993; *Doviak et al.*, 1996] to specify limits on the horizontal correlation lengths ρ_{Bx}, ρ_{By} of Bragg scatterers for which the echoing mechanism can be considered to be specular (i.e., reflective) or horizontally anisotropic or isotropic scatter (i.e., from horizontally anisotropic or isotropic refractive index perturbations). It is shown that the observed echoes reported here are due to a Fresnel scattering mechanism because the Bragg scatterers' correlation scales $\rho_{Bx,y}$ are not substantially smaller than the transmitting antenna diameter D [i.e., *Doviak and Zrnić*, 1993, condition (11.124)] and not larger than the first Fresnel zone diameter $2r_F$, which is the condition of reflection as shown in the appendix. Bragg scatterers are said to involve a Fresnel scattering mechanism if they have a sufficiently large cross-beam correlation length that requires second order expansion of the phase terms for closed form analytic solutions. If the correlation length is sufficiently small such that the second order expansion is not required, then the scattering mechanism is a Fraunhofer one [*Doviak and Zrnić*, 1993, section 11.5.2].

The paper is organized as follows. In section 2 we summarize the expressions needed to get the SA parameters. In section 3 the radar observations are presented, followed by a discussion in section 4. Finally, in section 5 our results are summarized.

2. SA Expressions for Calculating Scattering Parameters

Holloway et al. have shown that the magnitude of the normalized cross correlation function (NCCF) can be well approximated to have a Gaussian form. It is important to mention that Holloway et al.'s approach, based on assumptions about the scattering medium, and the approaches presented by *Briggs* [1984] and *Meek* [1980], based on assumptions about the diffraction pattern, each give essentially the same horizontal wind. However, Holloway et al. present explicit expressions to determine an indicator of tur-

Then we adopted a phase screen model for the refractive index of irregularities [*Ratcliffe*, 1956], i.e., bulent intensity of the wind and the parameters (orientation, shape, and sizes) of horizontally anisotropic perturbations of refractive index that scatter the incident radiation. Such parameters can be calculated as follows.

1. The indicator of turbulent intensity, σ_t (i.e., the standard deviation of assumed isotropic wind fluctuations within the radar's resolution volume), of an otherwise uniform flow is calculated using Holloway et al. (equations (34), (37), and (39)), i.e.,

$$\sigma_t = \left[\frac{1}{2k_0^2}\left(\frac{1}{2\tau_c^2} + 4Av_{0x}^2 + 4Bv_{0y}^2 + 8Hv_{0x}v_{0y}\right)\right]^{1/2} \quad (1)$$

where A, B, and H are parameters calculated from the magnitudes of the NCCFs [e.g., *Briggs*, 1984; *Holloway et al.*, 1997a], τ_c is the square root of the second central moment of the magnitudes of autocorrelation or cross-correlation functions, k_0 is the radar wavenumber ($2\pi/\lambda$), and v_{0x} and v_{0y} are the horizontally uniform wind components along the orthogonal x and y directions. A similar SA expression to infer an indicator of turbulent intensity (in this case the mean lifetime of the diffraction pattern) has been presented in previous works [e.g., *Briggs*, 1980, 1984].

The uniform velocity components can be obtained by using Holloway et al.'s (34) and (47) or by using other SA approaches [e.g., *Briggs*, 1984; *Meek*, 1980; *Briggs and Vincent*, 1992; *Sheppard and Larsen*, 1992; *Liu and Pan*, 1993]. A statistical comparison of horizontal winds obtained with most of these SA approaches has been presented by *Chau and Balsley* [1998c]. They found out that under a high SNR regime all the SA techniques studied gave, essentially, the same wind information. To estimate accurately the vertical component of wind, one needs to use the formulas presented by *Holloway et al.* [1998] or *Chau and Balsley* [1998a].

2. The angle of orientation of the irregularities (ψ) can be calculated from Holloway et al.'s (50); i.e.,

$$\psi = \frac{1}{2}\arctan\frac{2H}{A-B}. \quad (2)$$

3. The major and minor axes of the irregularities's correlation ellipse (ρ'_{Bx} and ρ'_{By}) are obtained from Holloway et al.'s (25); i.e.,

$$\rho'_{Bx} = \frac{\sqrt{\xi'^2_x - 2a_h^{-2}}}{2}, \quad (3)$$

$$\rho'_{By} = \frac{\sqrt{\xi'^2_y - 2a_h^{-2}}}{2}, \quad (4)$$

where ξ'_x and ξ'_y are the correlation lengths of the major and minor axes of the diffraction pattern along which the x' and y' axes are oriented. These correlation lengths can be obtained using Holloway et al.'s (52) and (51), respectively. The antenna parameter a_h, derived by *Doviak et al.* [1996], is given by

$$a_h \approx k_0\frac{\sigma_T}{z_0}\sqrt{\frac{2\sigma_R^2}{\sigma_T^2+\sigma_R^2}}, \quad (5)$$

where σ_T and σ_R, the beam widths in units of length at distance z_0, are the square roots of the second moments of the transmitting and receiving antenna's one-way radiation pattern, respectively. In the derivation of (5) the beams of the receiving and transmitting antennas are stipulated to have circular symmetry. We assume the square array antennas used in our experiment also produce circularly symmetric beams.

The correlation lengths of the scatterers can be used to calculate the components of the aspect sensitivity parameter θ_S [e.g., *Hocking et al.*, 1986]. The parameter θ_S provides a measure of the rate of fall off of power as a function of zenith angle, and it is usually obtained with SA systems. In previous papers a circularly symmetric backscatter polar diagram of the scatterers of the form $\exp[-\sin^2\theta/\sin^2\theta_S]$ has been assumed [e.g., *Reid*, 1988; *Holdsworth and Reid*, 1995; *Lesicar and Hocking*, 1992; *Lesicar et al.*, 1994], even though the scattering could have been horizontally anisotropic. It is possible to account for anisotropic scatter using the theory of *Briggs* [1992].

Taking into account the horizontally anisotropic case, the components of the aspect sensitivity vector (in radians) are calculated from

$$\theta'_{Sx} = \arcsin\frac{1}{\sqrt{2}k_0\rho'_{Bx}} \quad (6)$$

$$\theta'_{Sy} = \arcsin\frac{1}{\sqrt{2}k_0\rho'_{By}}. \quad (7)$$

In obtaining these expressions we employed the following polar diagram of backscatter:

$$B(\theta'_x,\theta'_y) \propto \exp\left[-\frac{\sin^2\theta'_x}{\sin^2\theta'_{Sx}} - \frac{\sin^2\theta'_y}{\sin^2\theta'_{Sy}}\right]. \quad (8)$$

$K_{x,y} = 2k_0 \sin\theta'_{x,y}$, and used it in a horizontally anisotropic version of the spatial spectrum of the refractive index of irregularities (see the isotropic version of *Doviak et al.* [1996, equation (28)]), to obtain an expression for the polar diagram of backscatter that has the horizontal correlation lengths explicitly shown. Moreover, in arriving at (6) and (7) we have assumed horizontal layers, i.e., $B(\theta'_x, \theta'_y)$, centered at $(0,0)$. However, these expressions do not get modified if layers with small tilt angles are considered [e.g., *Chau and Balsley*, 1998a]. We will be using (6) and (7) to compare observations of θ_S made by others to the observations reported in this paper.

3. Data Presentation

The Jicamarca radar (near Lima, Perú) operates at ~50 MHz and has a 288 by 288 m antenna array. The array is composed of 64 separate modules. Each module consists of a 12 by 12 array of cross-polarized half-wave dipoles. Figure 1 shows the antenna configuration for our measurements. The vertically pointing full array E was used for both transmission and reception (i.e., monostatic mode) in the x-aligned polarization to gather the information from the "narrow" vertical beam. Antenna D was also used in a monostatic mode in the y-aligned polarization to obtain the measurements from the "wide" vertical beam. Modules A, B, and C were pointed on axis (−1.46° from vertical along the y axis) and were used for reception only in the y-aligned polarization. Therefore the SA configuration consisted of receiving modules A, B, and C and the transmitting antenna D. As is shown by *Chau and Balsley* [1998a, section 2.1.2], the small off-vertical pointing of the receiving modules does not affect the magnitudes of the NCCFs because the one-way beam width of A, B, and C are much larger than the transmitting beam width. Note that the two-way half-power beam widths of the narrow and wide beams are ~0.8° and ~3.0°, respectively, and the one-way beam width of the receiving arrays A, B, and C is ~8.2°. More details on the experimental setup are given by *Chau and Balsley* [1998b].

We have obtained processed data every 196.6 s (~3 min). A Gaussian function has been fitted to the magnitude of the NCCFs, i.e., to the SA data. The amplitudes, delays to the peak (τ_p), and correlation widths (τ_c) of the Gaussian functions have been used to get the cross-correlation values at zero lag and the lags (τ_i) where the autocorrelation and the

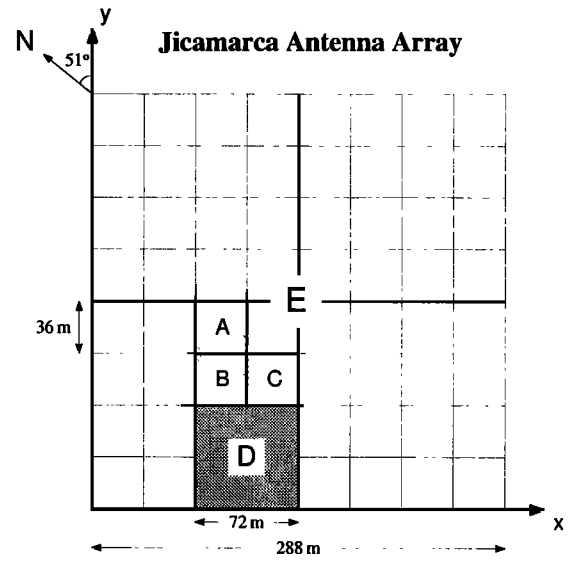

Figure 1. Antenna setup for the Jicamarca experiment. The full array, vertically pointing E module was used for transmission and reception in the x-aligned polarization. In the orthogonal polarization (y-aligned), the vertically pointing D module was used for transmission and reception, and the modules A, B, and C were used only for reception.

cross correlations intersect. Data have been rejected when (1) the signal to noise ratio (after coherent integration) was below -6 dB, (2) Gaussian fitting was poor, and (3) estimation of τ_c was not consistent (i.e., very different values of τ_c were obtained from the autocorrelations and the cross correlations). It is important to point out that we have removed "window biases" by dividing the NCCFs at lag k by $M - |k|$ instead of M [e.g., *Oppenheim and Schafer*, 1975, p. 554], where M is the number of points of the time series used. The spectral data from both vertically directed beams, wide and narrow, were analyzed using a least squares fitting approach similar to the one presented by *Sato and Woodman* [1982].

We present in Figure 2 the indicator of turbulent intensity and the diffraction pattern parameters obtained using Holloway et al.'s approach. In Figure 2a, we show the indicator of turbulent intensity σ_t calculated from (1), while the orientation of the diffraction pattern's correlation ellipse in the x, y coordinate frame is presented in Figure 2b. The orientation of the x, y coordinate frame is rotated clockwise by 51° relative to north (e.g., the x axis is at 141°, whereas the y axis is at 51° relative to north). We

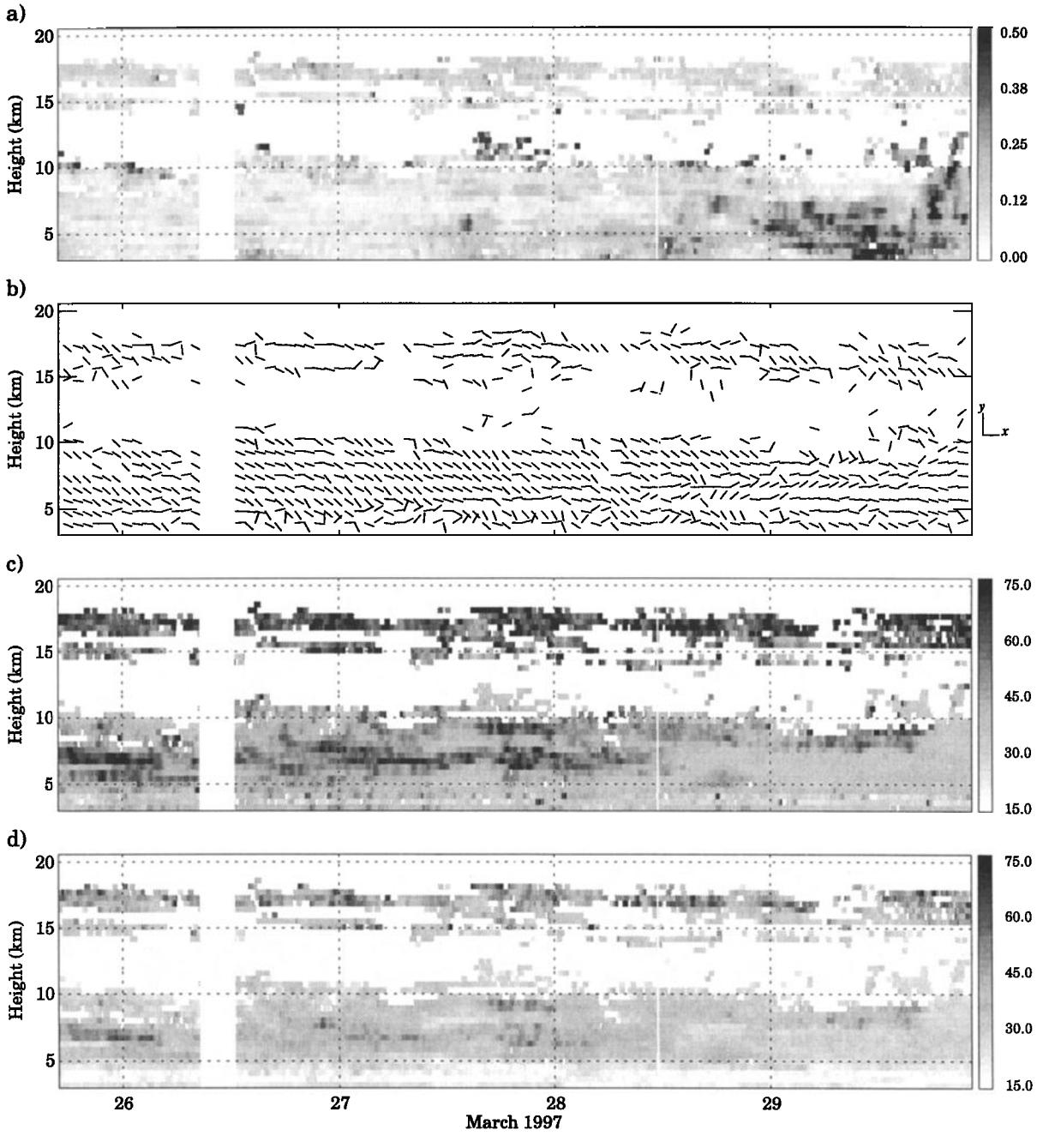

Figure 2. (a) Indicator of turbulent intensity σ_t, (b) orientation of the major axis of the diffraction pattern's correlation ellipse, and the correlation lengths (ξ'_x and ξ'_y) along the (c) major and (d) minor axes of the ellipse calculated using the spaced antenna (SA) configuration. The orientations are represented by short lines every 1 hour and 1 km, and horizontal and vertical lines are aligned with the x and y axes shown in Figure 1.

also present in Figures 2c and 2d the major and minor lengths of the diffraction pattern's correlation ellipse. In all cases we have applied a five-point median filter (~15 min) to each height in order to mask most of the outliers. On these diagrams, missing values have been represented in white, and they occur, mainly, above 10 km. When the "gaps" caused by the missing values were too long, we have used the original values instead of the filtered values.

Examining Figure 2, we can clearly identify space and time regions of weak and strong turbulence. Large regions of weak turbulence (i.e., $\sigma_t < 0.1$ m s^{-1}) occur on days 26 and 27, and at these locations, there is mostly a north-south orientation of the correlation ellipse and large values of the correlation length (i.e., $\xi'_{x,y} > 40$ m). On the other hand, regions of strong turbulence are mostly characterized by a random orientation of the correlation ellipse and much smaller values of correlation lengths.

To have a closer look at the relation between correlation lengths and the indicator of turbulent intensity, we present in Figure 3 a time series of these parameters at 6.60 km. Note that in Figures 3c and 3d we are also showing the values of the correlation lengths of the Bragg scatterers (ρ'_{Bx}, ρ'_{By}). Such values were obtained using an empirical value of the antenna parameter a_h in (3) and (4), respectively. Again, we see a long-lasting period of weak turbulence on day 27 and a long-lasting period of strong turbulence on day 29. Note some short transitional events of weak-strong-weak trubulence denoted by the pointing-up arrows, where a small increase of σ_t corresponds to a large decrease on both ξ'_x and ξ'_y. On the other hand, in strong-weak-strong transitional events of turbulence (e.g., the pointing-down arrow) a small increase on both correlation lengths is accompanied by a large decrease on σ_t. The median ratio ρ'_{By}/ρ'_{Bx} is 0.65. Slightly larger values are obtained above 15 km (~0.69).

The antenna parameter a_h, needed to get ρ'_{Bx} and ρ'_{By}, has been calculated from the observations in Figures 3c and 3d, and it is shown with a horizontal dashed line. We have chosen the minimum value of the smooth version (five-point median average) of the correlation lengths $\xi'_{x,y}$ in the region 5-8 km. This empirical value corresponds to $a_h \approx 0.052\text{m}^{-1}$. On the other hand, we have calculated the antenna beam widths from the theoretical antenna patterns of the coaxial-collinear (COCO) arrays used and applied them in (5) to obtain a theoretical value of 0.04 m^{-1}. The larger empirical value (~30%) implies that the actual antenna beam widths of the SA transmitting and receiving antennas are larger than the theoretical values that were computed assuming a uniform distribution of current across the arrays. These observations suggest that under certain conditions (i.e., $\rho_{Bx}, \rho_{By} \ll D$) we can use measured diffraction pattern scales to calculate the beam widths of the transmitting and receiving antennas.

To examine more thoroughly the negative correlation between the Bragg scatterer's correlation length and the indicator of turbulent intensity, we show in Figure 4 a scatter plot between ρ'_{Bx} and σ_t. Notice the L shape of the scatter plot for high values of σ_t, ρ'_{Bx} tends to a constant value (~12 m), while for low values of σ_t, ρ'_{Bx} has a broad range of relatively large values. The cause of the L-shaped pattern is discussed in section 4.3.

4. Discussion

4.1. Validity of SA Turbulence Measurements

What is the accuracy of the σ_t measurements? In order to get an approximated value we have calculated the autocovariance function of ~3 min σ_t values under two different turbulent conditions. In Figures 5a and 5b we show the time series and autocovariance function of σ_t for an 8 hour period of weak turbulence. The ~3 min estimates are represented by diamonds, while a three-point median average series is represented by a solid line in Figure 5a. The solid line in Figure 5b represents the autocovariance function for the solid curve in Figure 5a. Before the autocovariance function was calculated we removed the low-frequency components of both time series by subtracting a 20-point median average series. In Figure 5b, note the abrupt change in the autocovariance data from zero lag to the first lag and the more regular dependence for longer lags. At longer lags the autocovariance function exhibits a wave-like dependence with a 30 min period. This is likely due to the presence of a gravity wave. On the other hand, the abrupt change at zero lag suggests uncorrelated noise. An estimate of the error variance of σ_t is calculated by subtracting the autocovariance values of the two series (i.e., one with samples at 3 min inter-

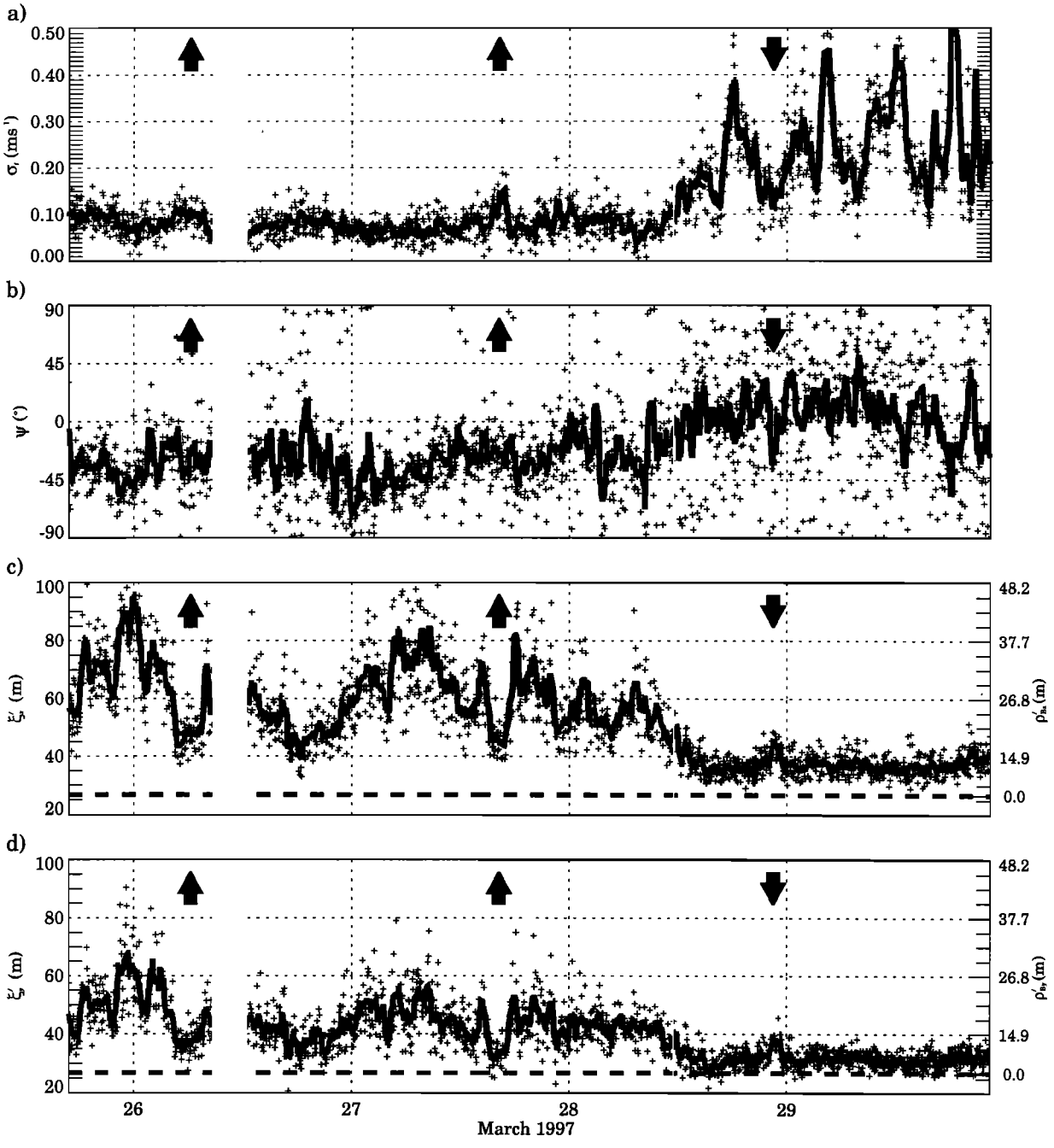

Figure 3. (a) Indicator of turbulent intensity, (b) angle ψ of orientation relative to the x axis in Figure 1, and (c) major and (d) minor correlation lengths at 6.6 km. The solid lines are five-point median averages. The arrows locate examples of weak-strong-weak (up) and strong-weak-strong (down) events of turbulence. The horizontal dashed lines on Figures 3c and 3d represent the antenna parameter ($\sqrt{2}a_h^{-1}$) that has been calculated from the ξ measurements.

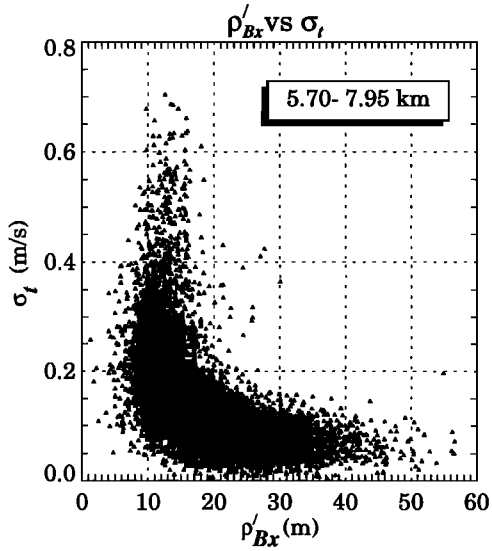

Figure 4. A scattered plot between ρ'_{Bx} and σ_t for heights 5.70-7.95 km.

vals and the other a three-point median average) at zero lag. The same procedure has been applied to an 8 hour period of strong turbulence in Figures 5c and 5d.

The computed values of the standard errors of the σ_t estimates are $\sim$1.4 cm s^{-1} and $\sim$5.0 cm s^{-1} for the periods of weak and strong turbulence. This corresponds to about an 18% relative error (i.e., relative to the mean value of σ_t) for both time periods. Therefore the calculated errors appear to be approximately proportional to the mean value of σ_t. This result is in agreement with theoretical statistical errors calculated for spectrum width measurements if the SNR is larger than $\sim$10 dB [*Doviak and Zrnić*, 1993, Figure 6.6].

We also compare the SA-calculated σ_t and the spectral widths σ_v observed with both vertical beams: wide and narrow (Figure 6). To be precise, we should compare σ_t calculated from σ_v. However, this calculation requires estimation of the Bragg scatterers'

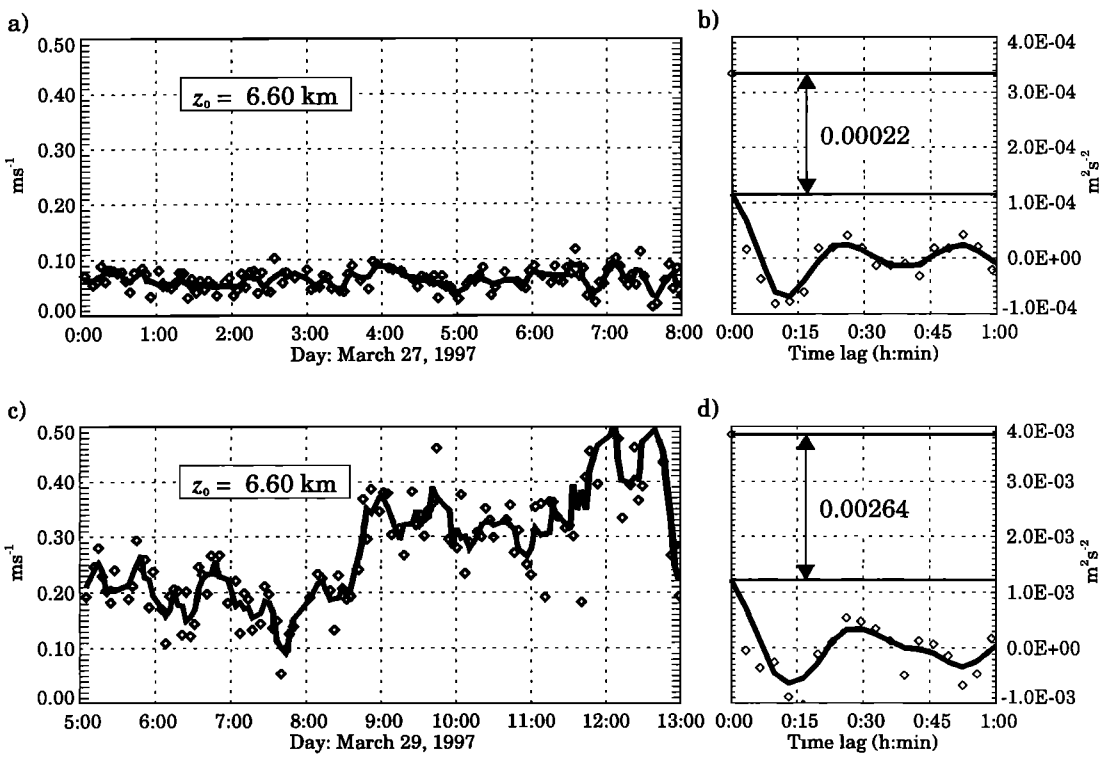

Figure 5. Time series and autocovariance function of σ_t, during periods of (a) and (b) weak and (c) and (d) strong turbulence. The diamonds represent the information for $\sim$3 min estimates, while the solid lines represent the information for the three-point median average. The empirical statistical error variances of σ_t are given by the difference between the two horizontal lines in Figures 5b and 5d.

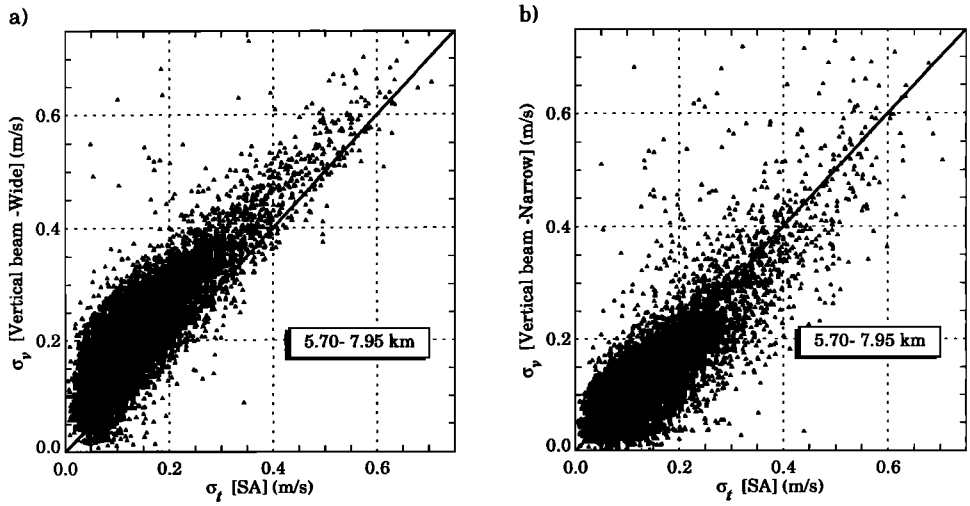

Figure 6. Comparisons of the SA indicator of turbulent intensity σ_t and the spectral width σ_v from two vertical beams: (a) wide (3.0°) and (b) narrow (0.8°).

correlation length. That is, using the vertical beams, the Bragg scatterers' horizontal correlation length must be known to estimate σ_t because Bragg scatterers having large horizontal correlation length and located nearer the beam axis will contribute much more to the backscattered signals than those scatterers nearer to the beam edge. This deduction is result of the fact that the diffraction pattern of Bragg scatterers with longer horizontal correlation lengths is narrower than the one produced by Bragg scatterers with shorter correlation lengths. Thus large Bragg scatterers not directly along the beam axis will contribute less backscatter than those away from it. In this case the region from where scatter is mostly returned to the receiving antenna is significantly less than the area illuminated by the transmitting beam. Consequently, the effect of uniform wind on spreading the Doppler spectrum of radial velocities is significantly reduced. This reduced effect is given by *Holloway et al.* [1997b, equation (36)]. For example, if the Bragg scatterers' correlation length is large, the correlation length of the diffraction pattern is correspondingly large, and hence the contribution σ_s to the spectrum width due to radial velocity shear of the uniform wind across the beam (i.e., the so called "beam broadening" effect) is less than if the scattering were isotropic. The condition for isotropic scattering from Bragg scatterers is given in the appendix. If scattering is isotropic, the smaller the beam width, the smaller the beam-broadening effect. Thus most accurate measurements of turbulence require the use of very narrow beams.

The SA method directly gives the horizontal correlation lengths of the Bragg scatterers that are needed to estimate σ_t using the vertical beam data. Doppler beam swinging (DBS) profilers typically have beams offset from the vertical at only a single zenith angle in two orthogonal directions. Thus there is at most a single point to estimate each of the horizontal correlation scales of the Bragg scatterers. This leads to much larger uncertainty in estimation of the correlation scales compared to that obtained with the SA method. This is particularly important for turbulence measurements with long wavelength (i.e., $\lambda > 1$ m) wind profilers. To obtain an accurate estimate of σ_t from the width σ_v of the observed Doppler spectrum, the contribution σ_s needs to be removed from σ_v, or very narrow beams should be used. There is an advection term due to vertical motions that also contributes to σ_v; this is typically small [*Doviak et al.*, 1996]. *Lesicar and Hocking* [1992] discuss a heuristic method to remove the beam-broadening effects, but the SA method of Holloway et al. automatically takes care of this effect.

Nevertheless, if the widths of the vertically directed beams are sufficiently narrow, the spectrum width σ_v will be a good estimate of σ_t. Thus, in Figure 6 we show scatter plots of σ_t versus σ_v ob-

tained from observations with both wide and narrow vertical beams, for the height interval 5.70-7.95 km. The wide beam values (Figure 6a) show larger values than σ_t because radial velocity shear across the beam, present even if wind is uniform, increases the spectrum width more for broader beams. We can clearly see the good agreement, as might be expected, between the σ_v measured with the narrow beam and σ_t obtained from Holloway et al.'s SA method.

The fact that we have good agreement between the spectrum width measured with the vertical beam of $\sim 0.8°$ width and the σ_t deduced from the SA configuration indicates that effects of radial velocity shear, associated with scales of motion larger than the resolution volume, are negligible in observations made with the narrow vertical beam. Thus the σ_t derived from SA observations, made with a transmitting beam width 4 times larger and receiving beams of widths 8 times larger than the narrow beam, should give reasonably accurate estimates of the turbulent component of vertical motions.

We now make some theoretical estimates of σ_t to compare to our observations. We assume that the variance of the turbulent velocity fluctuations, σ_t^2, can be written as twice the integral over the inertial range spectrum of the turbulent kinetic energy per unit mass [e.g., *Batchelor*, 1953, equations (3.1.6) and (6.5.3)]:

$$E(k) = \alpha \varepsilon^{2/3} k^{-5/3}, \tag{9}$$

where α is the so-called Kolmogorov constant, which has a universal value close to 1.5 [e.g., *Tatarskii*, 1971, section 12], ε is the energy dissipation rate per unit mass, and k is the wavenumber and where the integration is performed over all wavenumbers larger than a cut off wavenumber k_c:

$$\sigma_t^2 = 2 \int_{k_c}^{\infty} \alpha \varepsilon^{2/3} k^{-5/3} dk. \tag{10}$$

According to *Heisenberg* [1948, p. 635] the diameter d of a turbulent eddy is related to "its" wavenumber k via

$$k = \frac{\pi}{d}. \tag{11}$$

Equation (11) has been successfully applied for various problems in which it was necessary to relate geometrical properties of turbulence features in physical space to those in wavenumber space [e.g., *Muschinski and Roth*, 1993; *Muschinski*, 1996, p.245; 1998a, equation(2.11)]. Here we use (11) as a relation between the outer scale of the inertial subrange k_c and the diameter L of the largest overturning eddies:

$$k_c = \frac{\pi}{L}. \tag{12}$$

It is not certain whether or not L is necessarily identical to the thickness of the layer. By definition, however, the thickness of a turbulent layer is the upper limit of L within that layer. That is, when estimating σ_t on the basis of inertial range turbulence theory, we neglect contributions to the integral for σ_t^2 from wavenumbers smaller than k_c. Non overturning eddies are not expected to contribute to σ_t because in the free atmosphere, all vertical motions, except those associated with gravity waves, are part of the overturning process (i.e., turbulence); vertical motions on scales larger than L are associated with gravity waves or large-scale weather phenomena (e.g., fronts) that contribute only to the mean Doppler velocity; only vertical motions on scales smaller than σ_T (i.e., the beam width $\approx$100 m at $z = 6$ km) contribute to $\sigma_v = \sigma_t$ (Figure 6). Thus we obtain the following integral that relates σ_t, ε, and L:

$$\sigma_t^2 = 2 \int_{k_c}^{\infty} \alpha \, \varepsilon^{\frac{2}{3}} k^{-\frac{5}{3}} dk, \tag{13}$$

and we find

$$\sigma_t = \sqrt{3\alpha} \left(\frac{\varepsilon L}{\pi} \right)^{1/3} \approx 1.4 \, \varepsilon^{\frac{1}{3}} L^{\frac{1}{3}}. \tag{14}$$

This means that σ_t is a fairly weak function of ε. *Ball* [1961, Figure 3] has compiled ε measurements from 13 different sources into a single diagram that shows ε as a function of height in a log-log diagram. The altitudes range from <10 cm above the ground to well into the stratosphere. *Ball* [1961, Figure 3] shows that $\varepsilon = 10^{-5} \mathrm{m^2 s^{-3}}$ is a reasonable first guess for a representative value of ε in the middle troposphere. Then we obtain $\sigma_t = 3.2 \, \mathrm{cm \, s^{-1}}$ for $L = 1$ m and $\sigma_t = 15 \, \mathrm{cm \, s^{-1}}$ for $L = 100$ m. We conclude that the values for σ_t that we observed are in agreement with what one should expect from simple reasoning.

4.2. Observations of a Scattering Mechanism

We now show that our observations are due to a Fresnel scattering mechanism and not to a reflecting one. For this discussion we consider the height range 5.70-7.95 km, where the following parameters are obtained: (1) The first Fresnel zone radius r_F

is 130-154 m. (2) From Figure 4 the Bragg scatterers' correlation lengths along the major axis ρ'_{Bx} are 12-50 m. Slightly smaller values are obtained along the minor axis. These values of $\rho'_{Bx,y}$ correspond to aspect sensitivity values $\theta'_{sx,y}$ of 0.8°-14°. Similar values of θ'_s have been obtained in the 5-8 km region by *Vincent et al.* [1987] using the Adelaide VHF radar. Note that *Vincent et al.* [1987] assumed a horizontally isotropic aspect sensitivity function, i.e., $\exp[-\sin^2\theta/\sin^2\theta_S]$. (3) The median ratio ρ'_{By}/ρ'_{Bx} is 0.65.

Therefore, following the criteria presented in the appendix, our tropospheric observations come from a horizontally anisotropic scattering mechanism, i.e., $\min\{\rho'_{Bx,y}\} < 2r_F$ and $\rho'_{Bx} \neq \rho'_{By}$. Furthermore, because the Bragg scatterer's correlation length does not satisfy the condition $\rho_{Bx,y} \ll D/4$, the echoing mechanism is Fresnel scatter. Fresnel scatter arises because the second-order phase term is required in the scattering integral. The same result is obtained for the near-tropopause observations, although correlation scales are larger at those heights than at tropospheric heights (see Figures 2c and 2d).

4.3. Indicator of Turbulent Intensity Versus Bragg Scatterer's Correlation Length

An L-shaped pattern is found when values of σ_t are plotted against the horizontal scale ρ'_{Bx} of the Bragg scatterers (Figure 4; a similar L-shaped pattern is found when σ_t is plotted against ρ'_{By}). This suggests that if turbulence is extremely weak (i.e., $\sigma_t < 0.1$ m s^{-1}), the correlation scales have a large spread of relatively large values (i.e., up to 50 m), but if turbulence is strong, the correlation scales of the Bragg scatterers are much smaller.

During periods of strong turbulence the Bragg scatterers' correlation scales range from 6 to 15 m (Figure 4). If the Bragg wavelength places the radars sampling function in the isotropic region of the spectrum of refractive index perturbations [e.g., *Doviak et al.*, 1996, Figure 7], the Bragg scatterer's horizontal correlation length would be of the order of a wavelength [*Doviak et al.*, 1996, section 3.3]. Since the horizontal scales of refractive index perturbations during our observations of strong turbulence are of the order of a wavelength (i.e., 6 m), the scales of turbulence we observe during periods of strong turbulent activity are likely within the inertial subrange, which is the range of isotropic turbulence.

The presence of large correlation lengths when turbulence is extremely weak or absent suggests that the perturbations in refractive index are created upstream of the vertically directed antenna beam. We propose the following hypothetical scenario to explain this suggestion. After upstream turbulence smears (through the mixing process) the vertical gradient of the mean potential temperature in the mixed layer it enhances these gradients in regions bounding the mixed layer [e.g., *Muschinski and Wode*, 1998, Figure 8]. Within the regions of enhanced potential temperature gradients, refractive index perturbations are more intense, but buoyancy forces are stronger and more likely to attenuate the undulations of refractive index perturbations caused by turbulence and/or gravity waves within these regions. *Weinstock* [1978] demonstrates that gravity waves are excited by turbulence, and those with scales within the buoyancy subrange are weakly attenuated by turbulence, as they propagate away from the mixed layer, compared to those with scales in the inertial subrange. That is, turbulence both excites and attenuates gravity waves in the region bounding the nearly neutral layer being formed by the mixing action of turbulence. In strongly stratified (i.e., very stable) layers a wide spectrum of waves can propagate, but in weakly stratified layers, only longer waves can propagate. Thus the energy of the longer length gravity waves, excited by turbulence in the buoyancy subrange, can continue to propagate into the weakly stratified regions of the ambient atmosphere, whereas the smaller scales of turbulence and refractive index perturbations will be locally dissipated through the cascade process and eventually dissipated by molecular diffusion. In other words, the momentum and energy of turbulence within the buoyancy subrange can be carried away by gravity waves, leaving behind the horizontally large-scale perturbations of temperature and humidity that compose the perturbations of the refractive index. In summary the larger-scale velocity perturbations are reduced more quickly than those of the refractive index because internal waves in a stable environment transfer momentum but not heat or moisture, the two principal variables composing the refractive index field. Thus the cascade process for velocity could be a leaky one, whereby energy and momentum in the buoyancy and inertial subranges are transported away by internal waves as well as being transferred to smaller scales [e.g., *Bolgiano*,

1959]. In this way, large-scale velocity perturbations can be dissipated before those of the refractive index. These large-scale perturbations in the refractive index can then be only removed by molecular diffusion, a relatively slow process. For example, using equations developed by *Batchelor* [1953], *Muschinski* [1998b, p. 41] shows that the e-folding time for the decay of the 3 m refractive index scales observed with radar is ~80 min. Up to this point we only described how large-scale refractive index perturbations (i.e., Bragg scatterers) can remain after turbulence has ceased, but we do not explain why Bragg scatterers have smaller horizontal correlation lengths when turbulence is present. The following paragraph provides an explanation.

Bragg scatterers having large horizontal scales are not necessarily created by turbulence having the same scale as implied in the preceding discussion. That is, Bragg scatterers with large horizontal scales can be created by the vertical shear of horizontal wind [*Hocking and Hamza*, 1997]. Although turbulence has vanished (i.e., gravity waves carry away the perturbations of velocity while leaving behind those associated with refractive index), the remaining perturbations of refractive index are slowly stretched by vertical shear of the wind into horizontally elongated scattering and/or reflective structures. The farther upstream the source of turbulence, the more likely we would observe Bragg scatterers with large correlation lengths before they are dissipated by molecular diffusion. Moreover, while vertical shear of the wind horizontally elongates the perturbations of refractive index, it can be demonstrated that shear also sharpens their vertical gradients.

Our observations lead to the conclusion that in absence of turbulence above the radar site the horizontal scales of Bragg scatterers will most likely be the larger horizontal scales that remain after turbulence has ceased; the larger horizontal scales are continuously being generated by the action of vertical shear. These residual perturbations might be considered "fossil turbulence" because they are perturbations in the refractive index that remain after turbulence has ceased but often are thought to be those continually generated by active turbulence. However, the essential feature of fossil turbulence is that vertical velocity fluctuations are absent, although the horizontal motions might remain [*Woods*, 1969]. The σ_t we estimate comes from vertical motions within the radar's resolution volume, and these are the only ones measured with the vertical beam. Thus we cannot rule out that horizontal motions persist and that the original region of three-dimensional turbulence might have given way to two-dimensional turbulence. Nevertheless, refractive index perturbations appear to remain, although turbulence is very weak or absent.

5. Summary

This is the first time the Holloway et al. approach, which is based on assumptions about the scattering medium, is applied to a VHF SA system. With this approach, as with the FCA, beam-broadening effects are inherently removed, and we obtain direct measurements of the indicator of turbulent intensity. In addition, the orientation and sizes of horizontally anisotropic refractive index perturbations are also directly measured. These measurements have been obtained under two turbulent conditions: weak and strong.

The Holloway et al. approach provides reasonable mesurements of the indicator of turbulent intensity (σ_t). These values are in good agreement with concurrent values obtained with the Jicamarca vertically directed narrow beam (~0.8°). Furthermore, relative uncertanties of the SA σ_t measurements are ~18% for both periods of weak and strong turbulence, in agreement with theoretical expectations.

Our radar observations show that Bragg scatterers are horizontally anisotropic and that they form a Fresnel scattering process instead of a reflecting one (i.e., the horizontal correlation lengths are smaller than the first Fresnel zone). In addition, we report an L-shaped regression between Bragg scatterer's correlation lengths and indicators of turbulent intensity. That is, when turbulence is weak ($\sigma_t < 0.1$ m s^{-1}), the horizontal correlation lengths have a large spread of relatively large values (i.e., large aspect sensitivity), but when turbulence is strong, the horizontal correlation lengths are much smaller and roughly fixed at the radar wavelength. Finally, we suggest that the presence of large correlation lengths, when turbulence is weak, might be considered to be fossil turbulence.

Appendix: Discriminating Scatter and Reflection

Let us assume that the scattering or reflecting medium is uniformly advected and that only refractive index perturbations at the Bragg wavelength are

effective in returning signals to the receiver. DBS wind profilers determine whether the echoing mechanism is scatter or reflection by examining the angular dependence of the echo strength as a function of the beam's zenith angle. If the signal falls quickly as a function of zenith angle, the echoing mechanism is considered to be a reflecting one; decreasing quickly means that the effective width of the signal's zenith angle dependence approaches that of the transmitting antenna's beam width. If the width of this dependence on zenith angle is much larger than the transmitting antenna's beam width, the echoing mechanism is considered to be a scattering one.

However, if the wind profiler is a SA one, we cannot swing the beam to determine whether we have scatter or reflection. In this case, reflection is often distinguished from scatter by examining the fading time. If horizontally isotropic Bragg scatterers have a horizontal correlation length ρ_{Bh} sufficiently large, fluctuations in the backscatter power would vary slowly compared to that if ρ_{Bh} was considerably smaller. A scattering mechanism is considered to be acting if echoes vary rapidly, and a reflection mechanism is acting if signals do not vary or vary extremely slowly.

In either the DBS or SA methods, there are no assigned clear-cut critical values whereby one can distinguish scatter from reflection. *Doviak and Zrnić* [1984] prove that reflection is effective if the horizontal correlation length ρ_{Bh} is larger than the first Fresnel zone radius $r_F = \sqrt{\lambda z_0/2}$, where λ is the radar wavelength and z_0 is the range to the scattering or reflecting volume. *Doviak and Zrnić* [1984] show the equivalence between reflection and scatter formulas if the Bragg scatterers' correlation length is larger than the first Fresnel zone diameter. Many observations are in the antenna's far field, and in this region the first Fresnel zone radius is always smaller than the beam width. Thus there will likely be more than one Bragg scatterer across the beam even if reflection is the echoing mechanism. The fact that there could be several Bragg scatterers within the beam suggests a scatter mechanism and not a reflective one. Nevertheless, because most of the echoing power is usually returned from the first Fresnel zone, other Bragg scatterers within the beam but outside the first Fresnel zone do not contribute significantly to the returned power, and the echoing mechanism remains a reflecting one. The echoes are considered to be from a scattering mechanism only if $\rho_{Bh} < 2r_F$. On the other hand, even if $\rho_{Bh} > 2r_F$, a scattering mechanism could be considered to be in effect if many partially reflecting layers are randomly distributed in the vertical but lie within the radar's vertical resolution; that is, the reflecting layers are unresolved. This condition has been coined Fresnel scatter [*Gage et al.*, 1985]. Because the number of reflecting layers is a function of vertical resolution, the rapid fluctuations in the signal strength due to interference of echoes from many of the layers could vanish as the vertical resolution increased. Therefore we recommend that the term Fresnel scatter be applied only to conditions specified in the next paragraph.

Although the condition $\rho_{Bh} < 2r_F$ specifies that scattering is taking place, it can be shown, using the procedures outlined by *Doviak and Zrnić* [1993, section 11.5.2], that one must still expand the phase term in the scattering integral [*Doviak et al.*, 1996, equation (13)] to second order if ρ_{Bh} is not much less than $(a_h\sqrt{2})^{-1}$. Because $(a_h\sqrt{2})^{-1} \approx D/4$ (i.e., if receiving antenna size equals one half the transmitting antenna diameter D and the array elements are uniform excited), the Bragg scatterers' correlation lengths must be much smaller than the transmitting antenna in order to neglect the second-order expansion of the phase term in the scattering integral. Because $r_F > D$ in the far field of the antenna, there are conditions for which $\rho_{Bh} < 2r_F$ wherein scatter is from a collection of uncorrelated Bragg scatterers but yet the Fresnel term (i.e., due to the second-order expansion of phase) in the scattering integral must be included. Under these conditions we have Fresnel scatter [*Doviak and Zrnić*, 1993, section 11.5.2], but we need to distinguish this scatter from that if there are multiple unresolved reflecting layers having the condition $\rho_{Bh} > 2r_F$.

In conclusion, if the Bragg scatterers' horizontal correlation length ρ_{Bh} is larger than the diameter $2r_F$ of the first Fresnel zone (i.e., $\rho_{Bh} > 2r_F$), echoes are from a reflecting mechanism; if $\rho_{Bh} < 2r_F$ but equal to or larger than $\sim(a_h\sqrt{2})^{-1}$ (i.e., $\sim$14 m for $a_h = 0.05\text{m}^{-1}$ found in section 3), echoes are considered to be Fresnel scattered; if ρ_{Bh} is much less than $(a_h\sqrt{2})^{-1}$, we have Fraunhofer scatter [*Doviak and Zrnić*, 1993, section 11.5.2]; if the perturbations are horizontally anisotropic (i.e., $\rho_{Bx} \neq \rho_{By}$) but the maximum and minimum dimensions of their correlation ellipse both satisfy the conditions $(a_h\sqrt{2})^{-1} < \rho_{Bx}, \rho_{By} < 2r_F$, the diffraction pattern will retain the horizontal anisotropy of the scatterers [*Holloway*

et al., 1997a, equation (25)]; and if $\rho_{Bx}, \rho_{By} << (a_h\sqrt{2})^{-1}$, Bragg scatterers can be considered as discrete particles, and one cannot, from backscattered signal analysis alone, distinguish refractive index scatter from that scatter associated with discrete particles [*Doviak et al.*, 1994, section IV.3.6]. In this latter case, *Doviak et al.* [1996] give heuristic arguments showing that any anisotropy in the diffraction pattern is simply related to differences in the horizontal (x, y) dimensions of the transmitting antenna.

If the Bragg scatterers are horizontally anisotropic, the condition for scatter should be applied to the minor axis (i.e., $\min\{\rho_{Bx}, \rho_{By}\}$) of the Bragg scatterers' correlation ellipse. For example, if the echo is from a highly elongated Bragg scatterer for which $\max\{\rho_{Bx}, \rho_{By}\} > 2r_F$, the ensemble of these scatterers would constitute a scattering medium if $\min\{\rho_{Bx}, \rho_{By}\} < 2r_F$.

Acknowledgments. Part of this work has been supported by the National Science Foundation under grants ATM-9214657 and ATM-9614700. The authors thank Chris Hall (University of Tromsø) and an anonymous reviewer for their comments on the original manuscript.

References

Ball, F. K., Viscous dissipation in the atmosphere, *J. Meteorol.*, *18*, 553–557, 1961.

Batchelor, G. K., *The Theory of Homogeneous Turbulence*, Cambridge Univ. Press, New York, 1953.

Bolgiano, R., Jr., Turbulent spectra in a stably stratified atmosphere, *J. Geophys. Res.*, *64*, 2226–2229, 1959.

Briggs, B. H., Radar observations of atmospheric winds and turbulence: A comparison of techniques, *J. Atmos. Sol. Terr. Phys.*, *42*, 823–833, 1980.

Briggs, B. H., The analysis of spaced sensor records by correlation techniques, in *Handbook for the Middle Atmosphere Program*, pp. 166–186, Sci. Comm. on Solar-Terr. Phys. Secr., Univ. of Ill., Urbana, 1984.

Briggs, B. H., Radar measurements of aspect sensitivity of atmospheric scatterers using spaced-antenna correlation techniques, *J. Atmos. Sol. Terr. Phys.*, *54*, 153–165, 1992.

Briggs, B. H., and R. A. Vincent, Spaced-antenna analysis in the frequency domain, *Radio Sci.*, *27*, 117–129, 1992.

Chau, J. L., and B. B. Balsley, Interpretation of angle-of-arrival measurements in the lower atmosphere using spaced antenna radar systems, *Radio Sci.*, *33*, 517–533, 1998a.

Chau, J. L., and B. B. Balsley, A statistical comparison of VHF techniques to study clear-air vertical velocities in the lower atmosphere using the Jicamarca radar, *Radio Sci.*, *33*, 1565–1583, 1998b.

Chau, J. L., and B. B. Balsley, A statistical comparison of horizontal winds obtained by a variety of spaced antenna techniques using the Jicamarca radar, *Radio Sci.*, *33*, 1669–1683, 1998c.

Doviak, R. J., Scattering from refractive index perturbations in turbulent flow (stochastic Bragg scatter), in *Technical Report From the Indian Space Research Organization on Lectures From the School of Atmospheric Radar*, 76 pp., Sri Venkateswar Univ., Tirupati, India, 1999.

Doviak, R. J., and D. S. Zrnić, Reflection and scatter formula for anisotropically turbulent air., *Radio Sci.*, *19*, 325–336, 1984.

Doviak, R. J., and D. S. Zrnić, *Doppler Radar and Weather Observations*, 2nd ed., Academic, San Diego, Calif., 1993.

Doviak, R. J., R. J. Lataitis, C. L. Holloway, and J. S. Van Baelen, A generalized theoretical analysis of cross-correlation and cross-spectra for spaced antenna wind profilers, *Tech. rep.*, NCAR/TN-407+STR, 105 pp., Natl. Cent. for Atmos. Res., Boulder, Colo., 1994.

Doviak, R. J., R. J. Lataitis, and C. L. Holloway, Cross correlations and cross spectra for spaced antenna wind profilers, 1, Theoretical analysis, *Radio Sci.*, *31*, 157–180, 1996.

Gage, K. S., W. L. Ecklund, and B. B. Balsley, A modified Fresnel scattering model for the parametrization of Fresnel returns, *Radio Sci.*, *20*, 1492–1501, 1985.

Heisenberg, W., Zur statistischen Theorie der Turbulenz, *Z. Phys.*, *124*, 627–657, 1948.

Hocking, W. K., An assessment of the capabilities and limitations of radars in measurements of upper atmosphere turbulence, *Adv. Space Res.*, *17*, 37–47, 1996.

Hocking, W. K., and A. M. Hamza, A quantitative measure of the degree of anisotropy of turbulence in terms of atmospheric parameters, with particular relevance to radar studies, *J. Atmos. Sol. Terr. Phys.*, *59*, 1011–1020, 1997.

Hocking, W. K., R. Rüster, and P. Czechowsky, Absolute reflectivities and aspect sensitivities of VHF radio waves scatterers measured with the SOUSY radar, *J. Atmos. Sol. Terr. Phys.*, *48*, 131–144, 1986.

Holdsworth, D. A., and I. M. Reid, A simple model of atmospheric radar backscatter: Description and application to the full correlation analysis of spaced antenna data, *Radio Sci.*, *30*, 1263–1280, 1995.

Holloway, C. L., R. J. Doviak, and S. A. Cohn, Cross correlations of fields scattered by horizontally anisotropic refractive index irregularities, *Radio Sci.*, *32*, 1911–1920, 1997a.

Holloway, C. L., R. J. Doviak, S. A. Cohn, R. J. Lataitis, and J. S. V. Baelen, Cross correlations and cross spectra for spaced antenna wind profilers, 2, Algorithms to estimate wind and turbulence, *Radio Sci.*, *32*, 967–982, 1997b.

Holloway, C. L., R. J. Doviak, S. A. Cohn, J. L. Chau, and R. J. Lataitis, Determination of wind and scale of diffraction patterns of scatter from horizontally anisotropic refractive index irregularities, in *Procedings of the Eighth Workshop on Technical and Scientific Aspects of MST Radar*, pp. 53–56, Sci. Comm. on Solar-

Terr. Phys. Secr., Natl. Oceanic and Atmos. Admin., Boulder, Colorado, 1998.

Lesicar, D., and W. K. Hocking, Studies of seasonal behaviour of the shape of mesospheric scatterers using a 1.98 MHz radar, *J. Atmos. Sol. Terr. Phys.*, *54*, 295–309, 1992.

Lesicar, D., W. K. Hocking, and R. A. Vincent, Comparative studies of scatterers observed by MF radars in the Southern Hemisphere mesosphere, *J. Atmos. Sol. Terr. Phys.*, *56*, 581–591, 1994.

Liu, C. H., and C. J. Pan, New observational techniques for studying the dynamics of the middle atmosphere using the Chung Li VHF radar, *J. Atmos. Sol. Terr. Phys.*, *55*, 1055–1066, 1993.

Meek, C. E., An efficient method for analysing ionospheric drifts data, *J. Atmos. Sol. Terr. Phys.*, *42*, 835–839, 1980.

Muschinski, A., A similarity theory of locally homogeneous and isotropic turbulence generated by a Smagorinsky-type LES, *J. Fluid Mech.*, *325*, 239–260, 1996.

Muschinski, A., The mixing-angle hypothesis, *Contrib. Atmos. Phys.*, *71*, 273–280, 1998a.

Muschinski, A., The first moments of the variance- and cross-spectra of standard and interferometric clear-air Doppler-radar signals, *Tech. rep.*, NCAR/TN-407+STR, 102 pp., Natl. Cent. for Atmos. Res., Boulder, Colo., 1998b.

Muschinski, A., and R. Roth, A local interpretation of Heisenberg's transfer theory, *Contrib. Atmos. Phys.*, *66*, 335–346, 1993.

Muschinski, A., and C. Wode, First in-situ evidence for coexisting submeter temperature and humidity sheets in the lower free troposphere, *J. Atmos. Sci.*, *56*, 2893–2906, 1998.

Oppenheim, A. V., and R. W. Schafer, *Digital Signal Processing*, Prentice-Hall, Englewood Cliffs, N. J., 1975.

Ratcliffe, J. A., Some aspects of diffraction theory and their application to the ionosphere, *Rep. Prog. Phys.*, *19*, 188–267, 1956.

Reid, I. M., MF Doppler and spaced antenna radar measurements of upper middle atmosphere winds, *J. Atmos. Sol. Terr. Phys.*, *50*, 117–134, 1988.

Sato, T., and R. F. Woodman, Spectral parameter estimation of CAT radar echoes in the presence of fading clutter, *Radio Sci.*, *17*, 817–826, 1982.

Sheppard, E. L., and M. F. Larsen, Analysis of model simulations of spaced antenna/radar interferometer measurements, *Radio Sci.*, *27*, 759–768, 1992.

Tatarskii, V. I., The effects of the turbulent atmosphere on wave propagation, in *UDC 551.510*, 472 pp., U. S. Dep. of Comm., Washington, D. C., 1971.

Vincent, R. A., P. T. May, W. K. Hocking, W. G. Elford, B. H. Candy, and B. H. Briggs, First results with the Adelaide VHF radar: Spaced antenna studies of tropospheric winds, *J. Atmos. Sol. Terr. Phys.*, *49*, 353–366, 1987.

Weinstock, J., On the theory of turbulence in buoyancy subrange of stably stratified flows, *J. Atmos. Sci.*, *35*, 634–649, 1978.

Woods, J. D., Fossil turbulence, *Radio Sci.*, *4*, 1365–1367, 1969.

J. Chau, Radio Observatorio de Jicamarca, Apartado 13-0207, Lima, Peru (chau@geo.igp.gob.pe)

R. Doviak, NOAA National Severe Storms Laboratory, 1313 Halley Circle, Norman, OK 73069.

C. Holloway, Institute for Telecommunications Sciences, National Telecommunications and Information Administration, Boulder, CO 80303.

A. Muschinski, Cooperative Institute for Research in Environmental Sciences, University of Colorado, Boulder, CO 80303.

(Received February 8, 1999; revised September 20, 1999; accepted October 13, 1999.)